


Spring 6-4-2015

Temperature Dependent Surface Reconstruction of Freely Suspended Films of 4-n-heptyloxybenzylidene-4-n-heptylaniline

Daniel E. Martinez Zambrano
Lawrence University

Follow this and additional works at: <https://lux.lawrence.edu/luhp>

 Part of the [Condensed Matter Physics Commons](#), [Other Materials Science and Engineering Commons](#), [Other Physical Sciences and Mathematics Commons](#), [Polymer and Organic Materials Commons](#), [Statistical, Nonlinear, and Soft Matter Physics Commons](#), and the [Structural Materials Commons](#)

© Copyright is owned by the author of this document.

Recommended Citation

Martinez Zambrano, Daniel E., "Temperature Dependent Surface Reconstruction of Freely Suspended Films of 4-n-heptyloxybenzylidene-4-n-heptylaniline" (2015). *Lawrence University Honors Projects*. 81.
<https://lux.lawrence.edu/luhp/81>

This Honors Project is brought to you for free and open access by Lux. It has been accepted for inclusion in Lawrence University Honors Projects by an authorized administrator of Lux. For more information, please contact colette.brautigam@lawrence.edu.

LAWRENCE UNIVERSITY

**Temperature dependent surface
reconstruction of freely suspended films
of 4-n-heptyloxybenzylidene-4-n-
heptylaniline**

by

Daniel Martinez Zambrano

A thesis submitted in partial fulfillment for the
Honors Project

June 2015

Declaration of Authorship

I, DANIEL MARTINEZ ZAMBRANO, declare that this thesis titled, ‘TEMPERATURE DEPENDENT SURFACE RECONSTRUCTION OF FREELY SUSPENDED FILMS OF 4-N-HEPTYLOXYBENZYLIDENE-4-N-HEPTYLANILINE’ and the work presented in it are my own. I confirm that:

- This work was done wholly or mainly while being a student at this university.
- Where any part of this thesis has previously been submitted for an honors project or any other qualification at this university or any other institution, this has been clearly stated.
- Where I have consulted the published work of others, this is always clearly attributed.
- Where I have quoted from the work of others, the source is always given. With the exception of such quotations, this thesis is entirely my own work.
- I have acknowledged all main sources of help.
- I have made clear exactly what was done by others and what I have contributed myself.

Signed:

Date:

“Nothing happens until something moves.”

–Albert Einstein

Abstract

by [Daniel Martinez Zambrano](#) and [Jeffrey Collett](#)

Surfaces of freely suspended thick films of 4-n-heptyloxybenzylidene-4-n-heptylaniline (7O.7) in the crystalline-B phase have been imaged using non-contact mode atomic force microscopy. Steps are observed on the surface of the film with a height of 3.0 ± 0.1 nm corresponding to the upright molecular length of 7O.7. In addition, we find that the step width varies with temperature between 56 °C and 59 °C. The steps are many times wider than the molecular length, suggesting that the steps are not on the surface but instead originate from edge dislocations in the interior. Using a strain model for liquid crystalline layers above an edge dislocation to estimate the depth of the dislocation, we estimate that the number of reconstructed surface layers decreases from 50 to 4 layers as the temperature increases from 56 °C to 59 °C. This trend tracks the behavior of the phase boundary in the thickness dependent phase diagram of freely suspended films of 7O.7, suggesting that the surface may be reconstructed into a smectic-F phase.

Acknowledgements

I would like to express my special appreciation and thanks to my advisor professor Jeffrey Collett; you have been a tremendous mentor. I want to thank you for encouraging my research and for allowing me to grow as a research scientist. Your advice on both research as well as on my career have been priceless. I would also like to thank professor John Brandenberger for motivating me and for suggesting ways to improve my work throughout my time at Lawrence. In addition, I would like to thank Mr. LeRoy Frahm for his technical expertise and substantial help in the lab improving the experimental design. Finally, I want to acknowledge the Excellence in Science Fund for allowing me to perform professional condensed matter research for two consecutive summers at Lawrence. Without the financial support, none of this would have been possible.

I also want to mention previous student researchers that have worked with professor Jeffrey Collett, such as Chris Hawley and Hannah Gabriel. Chris Hawley did outstanding work improving the experimental apparatus, and Hannah Gabriel studied the theoretical aspect of liquid crystal dislocations. Their contributions were very important to the project and present study.

Contents

Declaration of Authorship	i
Abstract	iii
Acknowledgements	iv
List of Figures	vi
1 Liquid crystals and 7O.7	1
1.1 What are liquid crystals?	1
1.2 Properties of liquid crystals	2
1.3 4-n-heptyloxybenzylidene-4-n-heptylaniline (7O.7)	4
2 Surface structure predictions	7
2.1 Previous work done on 7O.7	7
2.2 X-ray diffraction simulation	9
3 Experimental techniques	15
3.1 Atomic force microscopy techniques	15
3.2 Liquid crystal film assembly	18
3.3 Temperature control	19
3.4 Calibration samples and limits of the AFM	20
4 Experimental results	22
4.1 In search of the modulated surface	22
4.2 Molecular steps	24
4.3 Temperature-dependent step width	25
5 Data analysis and conclusions	28
5.1 Dislocation theory	28
5.2 Model	29
5.3 Depth of surface phase vs. temperature	32
5.4 Conclusions	33
References	35

List of Figures

1.1	Phase diagram of a conventional liquid crystal	3
1.2	7O.7 molecule shape	4
1.3	Thickness dependent phase diagram	5
1.4	Phases in thick films	5
1.5	Surface possibilities	6
2.1	Possible surface shapes for the Hex-AAA phase	8
2.2	X-ray data from Sirota	9
2.3	Reciprocal hexagonal lattice	10
2.4	Simulation results 1	12
2.5	Simulation results 2	12
2.6	Simulation results 3	13
2.7	Predictions from x-ray data	14
3.1	AFM interaction plots	17
3.2	AFM cartoon	17
3.3	Film assembly	18
3.4	AFM pictures	20
3.5	Silicon carbide data	21
4.1	Featureless surface	23
4.2	Smectic-F and smectic-A	23
4.3	Single step	24
4.4	Step profiles	25
4.5	Step width vs. temperature	26
4.6	Surface model	26
5.1	Crystal and liquid crystal dislocations	29
5.2	Dislocation extremes	30
5.3	Cartoon model	31
5.4	Liquid crystalline configuration	32
5.5	Surface depth vs. temperature	33

Chapter 1

Liquid crystals and 70.7

We start with a brief introduction to liquid crystals and discuss where they are found both in nature and industry. We then delve into the structure of liquid crystalline phases to explain their interesting optical and biological properties. The last part of this chapter discusses the molecule of interest and the main question we want to address.

1.1 What are liquid crystals?

Liquid crystals are ubiquitous. They are organic molecules that are integral to biological processes inside our bodies and are also found in high-definition displays. Cholesterol, for example, is a liquid crystalline molecule that is essential to the structure of cell membranes to maintain integrity and fluidity in cell transport. Some organisms, such as jewel beetles, exhibit liquid crystalline skin membranes that allow them to reflect light with brilliant metallic colors[1]. This is due to the so-called helical structure of the liquid crystal membrane. When the “size” of the helix is comparable to the wavelength of visible light, beautiful optical properties emerge. DNA and many polypeptides can also behave as liquid crystals under certain conditions. Such molecules are vital to processes such as cell division and transmission of genetic information. For this reason, liquid crystalline systems constitute an important part of current academic research.

Liquid crystals are also chemically synthesized. Although liquid crystals found in nature are critical to biological processes, their properties are also vital to the manufacture of high quality instrumentation and displays. Chemically synthesized liquid crystals are used to make spatial light modulators (SLMs) that modulate the amplitude, phase, or polarization of light waves in space and time. Applications of such devices range from high quality micro-mirrors, to different scanning and printing technologies[2]. Synthetic

liquid crystals are also used to manufacture high-definition displays. Currently, the production of liquid crystal displays (LCDs) is the most widely used application of liquid crystalline materials. Each pixel of an LCD consists of a layer of liquid crystals aligned between two transparent electrodes and two polarizing filters. By applying an electric field to the pixel (in the form of a voltage), it is possible to change the orientation of the molecules. As a consequence, it is possible to block or allow light to pass through the pixel. Programming specific voltages to the entire array of pixels can then create an image for the viewer. Liquid crystals are a great medium for displays because they excel at many important display properties, such as contrast ratios and switching times, compared to other mediums[3]. In general, they are also quite efficient and consume less power at high brightness settings compared to newer LED displays.

More importantly, liquid crystals have been popular in physics research for the past century due to their unique molecular ordering. Condensed matter physics is deeply concerned with the nature of phase transitions and scientists have always been trying to understand how matter organizes itself. Liquid crystalline materials have been studied due to their unconventional structure and phase changes at the molecular level. Understanding the structure of such phase changes is important to answer fundamental questions regarding the nature of phase transitions.

1.2 Properties of liquid crystals

All substances can exist in more than one state of matter. Water, for example, is a solid below 0 °C, a liquid between 0 °C and 100 °C, and a gas above 100 °C. Although these are the most common states of matter, they are not the only ones that exist. In addition to these states, there are a wide array of molecules that exhibit intermediate phases between liquid and solid. Regular solids consist of a rigid arrangement where each molecule occupies a certain place in the arrangement. This arrangement is usually periodic in nature, and scientists represent the repeating structure with a so-called lattice space. A liquid, on the other hand, does not exhibit this periodic arrangement. The molecules in a liquid are randomly dispersed throughout the material. As the name suggests, liquid crystals exhibit a combination of crystalline and liquid properties. Liquid crystals have some sort of organization, but they do not form a complete 3D lattice. The smectic phases, for example, are liquid crystalline phases in which the molecules stack themselves in layers, but within each layer, the molecules are free to move in random directions while still maintaining a particular orientation[3]. Fig. 1.1 shows a phase diagram of a liquid crystal molecule.

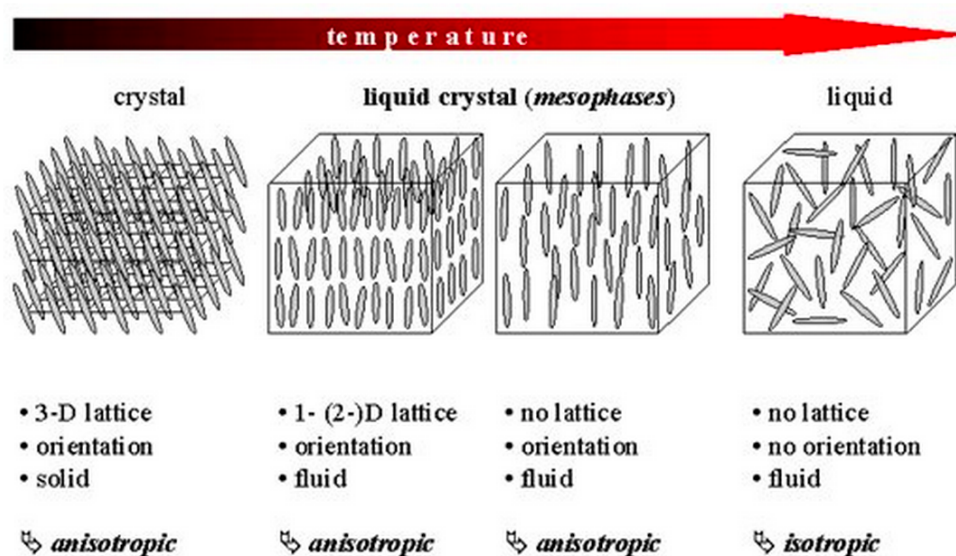


Figure 1.1: Phase diagram of a conventional liquid crystal molecule. Note that the mesophases (or the liquid crystal phases) have fluid properties as well as molecular orientation. The smectic phases form layers in addition to orientation. *Reprinted from [4].*

The crystal phase in the far left of Fig. 1.1 forms a 3D lattice where all the molecules point in a particular direction. This phase also has anisotropic properties, meaning that the crystal looks different when viewed in different directions due to the orientation of the molecules. After heating the crystal phase by a small amount, the rigid ordering transforms into a less rigid liquid crystalline ordering where the molecules form a fluid layered structure. Within each layer, the molecules are free to move in random directions while still maintaining a particular orientation. This phase is called smectic-A, and it is shown to the right of the crystal phase in Fig. 1.1 (the “A” means that the molecules are oriented perpendicular to the layers). After heating the smectic-A phase, the molecules enter the nematic phase in which the layer ordering disappears and only the molecular orientation persists. The nematic phase is shown to the right of the smectic-A phase in Fig. 1.1. After heating the nematic phase, the molecules are no longer oriented and the system enters the isotropic liquid phase. In this phase, the molecules are free to move in all possible directions and there is no tendency to maintain a particular orientation. This last phase resembles the structure of water.

1.3 4-n-heptyloxybenzylidene-4-n-heptylaniline (7O.7)

We have investigated a liquid crystalline material called 4-n-heptyloxybenzylidene-4-n-heptylaniline. For conciseness, we will refer to this material as simply 7O.7. Fig 1.2 shows a model of the molecular shape and composition of 7O.7.

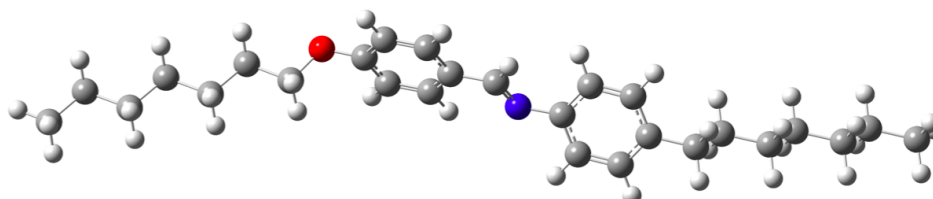


Figure 1.2: Simulated molecular shape and composition of 7O.7. Color code: gray (carbon), white (hydrogen), red (oxygen), blue (nitrogen).

The upright molecular length of 7O.7 has been experimentally measured and has a value of 3.05 nm[5]. The width of the molecule is close to 0.5 nm. Due to the geometrical shape of the molecule, the reader can think of 7O.7 as a cigar-shaped molecule with a rigid center attached to a pair of flexible hydrocarbon tails.

7O.7 has a rich phase structure. In a narrow temperature range, 7O.7 goes through various second-order phase transitions in which the ordering of the molecules changes by a significant amount. In 1987, Sirota *et al.* reported the phases and ordering structure of 7O.7 films in this narrow temperature range[5]. In addition to the drastic changes in molecular ordering, the phases also depend on the number of layers of the sample. That is, the thickness of the sample will dictate which phases are going to be present. Fig. 1.3 depicts the thickness dependent phase diagram of 7O.7 as a function of temperature.

The crystalline phases of 7O.7 in this temperature range are quite peculiar. Conventional crystal structures form a periodic lattice where the arrangement of the atoms or molecules is dictated by the geometry of the unit cell. Unit cells can have cubic, hexagonal, or orthorhombic structures, just to name a few. Interestingly, in addition to the usual lattice structure that most crystals have, 7O.7 also exhibits modulated phases. These modulated phases have static modulations with fixed spacial frequencies and amplitudes in addition to the regular crystal structure. The modulations are frozen in space and do not change with time.

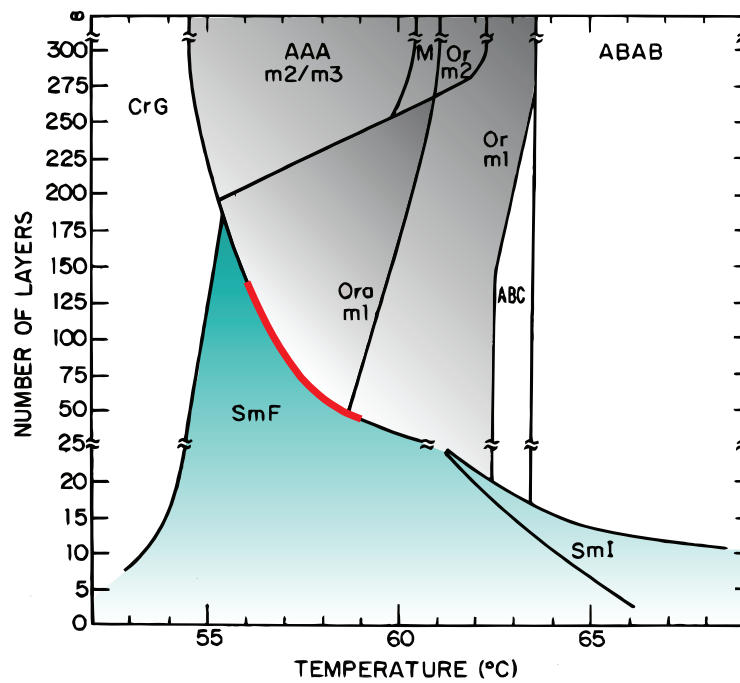


Figure 1.3: Thickness dependent phase diagram of 7O.7 as a function of temperature. The shaded area in gray represents modulated crystalline phases. The shaded blue-greenish area represents smectic liquid crystalline phases. Non-shaded areas are conventional (non-modulated) hexagonal crystal structures. The red curve highlights the temperature region we have investigated. *Adapted from* [5].

For this investigation, thick films of at least 30 micrometers (about 10,000 layers or more) were made. As a consequence, not all of the phases depicted in the phase diagram in Fig. 1.3 are allowed in the interior of the film. The particular phases that are present in our films are shown in Fig. 1.4.

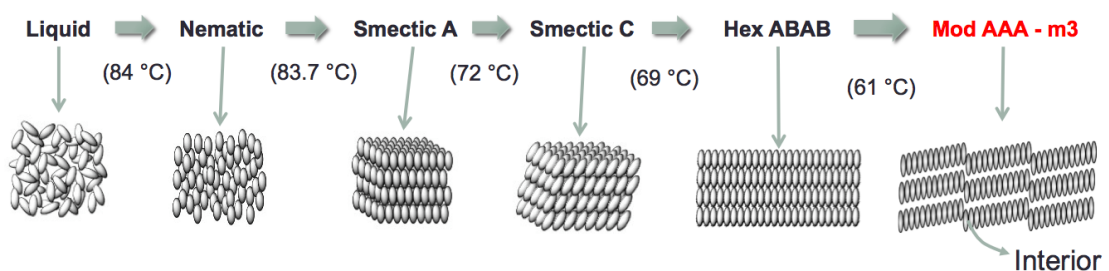


Figure 1.4: Some of the 7O.7 phases present in the interior of thick films. Both smectic phases and the nematic phase are liquid crystalline phases. The Hex ABAB and the Mod AAA-m3 phase are hexagonal crystalline phases. Note the modulated structure of the Mod AAA-m3 phase.

For thin films, on the other hand, the modulated crystal phases are not present according to the phase diagram in Fig. 1.3. Instead, the modulated phases are replaced by the smectic-F and smectic-I liquid crystalline phases. For a thin film (≈ 20 molecular layers) at 56°C , we encounter a smectic-F ordering. Yet, at that same temperature, we encounter the modulated hexagonal AAA phase in the interior of thick films (≈ 275 molecular layers). This discussion motivates the main question we want to address: What phase do we observe on the surface of thick films of 7O.7? Is the surface behaving as a thin film, or is it the same as the modulated crystalline interior? If the surface is behaving as a thin film, we should expect a surface reconstruction where the modulated crystal phase gets replaced by a liquid crystalline phase because the phases in thin films differ from the phases in thick films. If there is no reconstruction, we should expect the same modulated crystal structure that is found in the interior. Fig. 1.5 illustrates the two possibilities for the surface structure of 7O.7 between 56°C and 59°C .

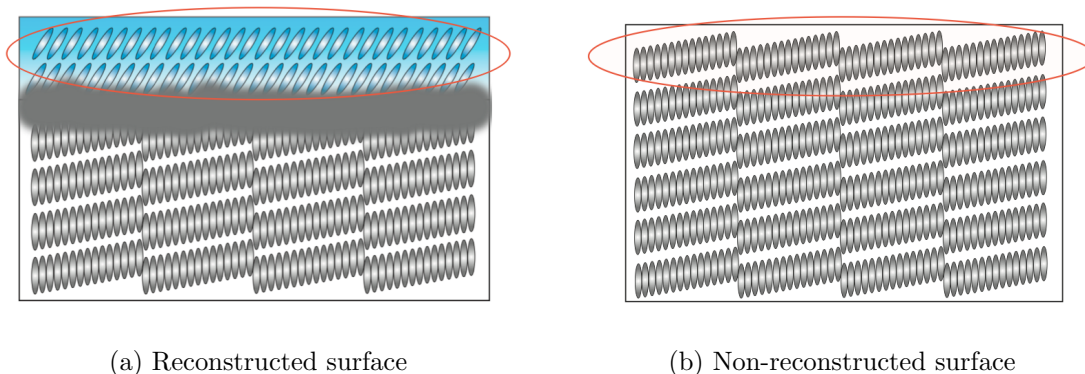


Figure 1.5: Surface possibilities for 7O.7 between 56°C and 59°C . Note that the surface of possibility (a) reconstructs into a phase that differs from the interior. Possibility (b) does not involve a reconstruction. Instead, the surface structure is the same as the interior crystalline structure.

There are many natural questions that arise if the surface of 7O.7 reconstructs. For example: What phase is the surface reconstructing into? Is it a liquid crystalline or a non-liquid crystalline phase? How thick is the reconstructed layer? As we will see in the following chapters, the surface of 7O.7 reconstructs. We will address the other questions in subsequent chapters because they are vital to this investigation. In order to understand whether the surface reconstructs, we need a detailed understanding of features of an unreconstructed surface.

Chapter 2

Surface structure predictions

Before we discuss the experimental techniques used to probe the surface of 7O.7, we must motivate why such methods are suitable in the first place. In the first part of this chapter we discuss past work that has been done on 7O.7 and utilize previous results to model the structure of an unreconstructed surface. We will then use this model to predict the surface features we should expect if the surface does not reconstruct.

Non-contact atomic force microscopy (NC-AFM) will be used to image the surface of freely suspended films of 7O.7. The instrument is sensitive to changes on the order of 0.1 nm in the vertical direction perpendicular to the sample. The lateral resolution in the plane of the sample is on the order of 4 – 5 nm, which is dictated mostly by the sharpness of the tip of the AFM. The predicted surface features we will find are well within the resolution of the instrument.

2.1 Previous work done on 7O.7

Previous x-ray studies indicate that some crystalline phases of 7O.7 are modulated^[5]. In the temperature range of interest (56 °C - 59 °C), thick films of 7O.7 form a hexagonal-AAA m2/m3 crystal structure. Each word of the name describes a specific attribute of the phase: hexagonal stands for the conventional hexagonal molecular ordering. That is, thick films of 7O.7 form a hexagonal lattice in this temperature range. The “AAA” indicates the stacking of the layers where each molecule is directly above a molecule from the layer below. The “m2/m3” indicates the modulated structure. If the film is quenched (that is, if the film is cooled rapidly) we obtain the “m3” modulated structure. On the other hand, if the film is cooled slowly we obtain the “m2” modulated structure. The m2 and m3 differ only in direction. Both modulations are two-dimensional, meaning

that there are two wave vectors in two different directions. In the m2 phase, the wave vectors are 45° apart, while in the m3 phase, the wave vectors are 90° apart. Fig. 2.1a illustrates a modulated layer where the wave vectors \mathbf{q}_1 and \mathbf{q}_2 are 90° apart. Note that the direction of the modulation is strictly in the plane of the layers and the displacements are perpendicular to the layers.

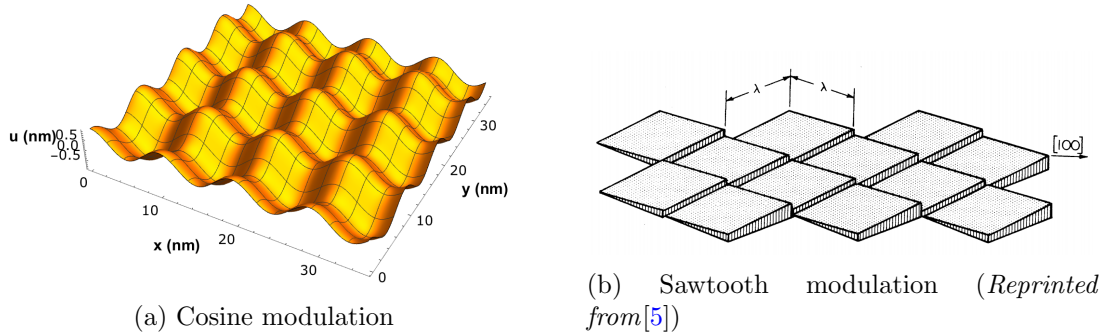


Figure 2.1: Modulated structure of the Hex-AAA m2 and m3 phase. (a) cosine modulation for the Hex-AAA m3 where the wave vectors $\mathbf{q}_1 = q_x \hat{\mathbf{x}}$ and $\mathbf{q}_2 = q_y \hat{\mathbf{y}}$ are 90° apart. (b) proposed sawtooth modulation for the Hex-AAA m2 phase where the wave vectors are 45° apart (the $[100]$ direction is the $\hat{\mathbf{y}}$ direction).

If the modulation were to be present at the surface (which corresponds to the non-reconstructed surface depicted in Fig. 1.5b), it is important to obtain concrete predictions for the attributes of the modulation, such as the spatial frequency and amplitude. In order to successfully predict these values, we must analyze the data from the x-ray studies that confirm the existence of the modulated phases.

In the narrow temperature range of interest ($56^\circ\text{C} - 59^\circ\text{C}$), x-ray studies indicate the existence of the modulation by the appearance of extra peaks in reciprocal space [5]. In addition to the main Bragg peak from the hexagonal structure, there are also four neighboring peaks surrounding the main peak. Two of these surrounding peaks (or “satellite” peaks) represent the modulation in the x-direction and the other two represent the modulation in the y-direction. In some phases at higher temperatures, only one pair of satellite peaks is observed; in this case the modulation is 1-dimensional. Fig 2.2 shows the x-ray data acquired by Sirota *et al.* in 1987 [5]. Fig. 2.2a illustrates one of the scans in reciprocal space of the Hex-AAA m3 phase. Note that there are three peaks in this plot: the main (001) Bragg peak at $q = 0$, and the two satellite peaks at $q = \pm 0.046$ in units of $4\pi/\sqrt{3}a$. The scaling factor of $4\pi/\sqrt{3}a$ comes from the in-plane nearest neighbor distance in reciprocal space. The other two satellite peaks are not shown because Fig. 2.2a only plots one slice of reciprocal space. A density plot is required to visualize both pairs of satellite peaks.

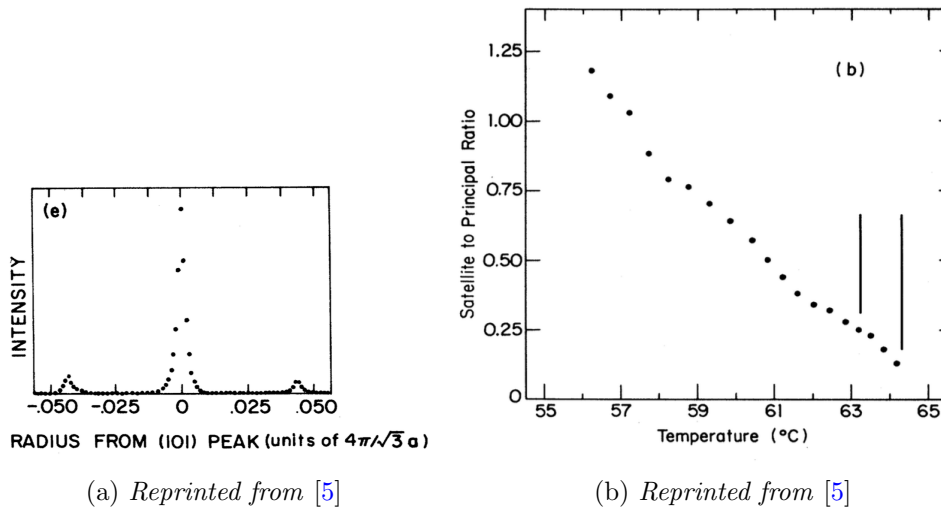


Figure 2.2: X-ray data from Sirota *et al.* indicating the existence of the modulation and its dependence with temperature. (a) main (001) Bragg peak at $q = 0$ with symmetric satellite peaks at $q = \pm 0.046$ in units of $4\pi/\sqrt{3}a$. (b) temperature dependence of the ratio between the maximum value of the main Bragg peak and the maximum value of the satellite peak.

The plot in Fig. 2.2b illustrates one of the most important results of 70.7's molecular structure. As the temperature decreases, the satellite to main peak ratio increases. The satellite to main peak ratio is related to the amplitude of the modulation. In particular, as the ratio increases, the amplitude of the modulation increases. This means that as the temperature decreases, the amplitude of the modulation increases. In order to uncover how the actual amplitude of the modulation varies with temperature, we must perform a numerical x-ray simulation to assign an amplitude to each satellite to peak ratio.

2.2 X-ray diffraction simulation

From Fig. 2.2a it is clear that the spacing between the main (001) peak to one of the satellites is 0.046 in units of $4\pi/\sqrt{3}a$. Previous experiments have determined that the lattice constant is equal to $a = 5.05 \text{ \AA}$ corresponding to the in-plane nearest neighbor distance in real space[6]. Using both of these values, we obtain a wavelength of 13.4 nm for the modulation. The spacing between the main (001) peak and the satellite peak perpendicular to the one in Fig. 2.2a also has a value of 0.046[5]. In order to relate the results from Sirota *et al.* to actual amplitude values for the modulation, we must relate the structure of the Hex-AAA phase to the amplitude of the modulation. To simplify the calculations, we assume that the lattice is made up of point scatterers instead of elongated liquid crystals. Other factors, such as Debye-Waller effects, will be neglected as well.

We begin with a hexagonal lattice given by the crystal axes

$$\mathbf{a}_1 = a \hat{\mathbf{x}} \quad \mathbf{a}_2 = \frac{1}{2}a \hat{\mathbf{x}} + \frac{\sqrt{3}}{2}a \hat{\mathbf{y}} \quad \mathbf{a}_3 = c \hat{\mathbf{z}}$$

where any point in the real lattice has the form $\mathbf{R}_{n,m,p} = n \mathbf{a}_1 + m \mathbf{a}_2 + p \mathbf{a}_3$ ($n, m, p \in \mathbb{Z}$). We set $a = 5.05 \text{ \AA}$, which corresponds to the nearest neighbor distance of 70.7 according to the x-ray data, and we set $c = 3.05 \text{ nm}$, which corresponds to the upright molecular length of 70.7[6]. The reciprocal vectors are given by

$$\mathbf{b}_1 = \frac{2\pi}{a} \hat{\mathbf{x}} - \frac{2\pi}{\sqrt{3}a} \hat{\mathbf{y}} \quad \mathbf{b}_2 = \frac{4\pi}{\sqrt{3}a} \hat{\mathbf{y}} \quad \mathbf{b}_3 = \frac{2\pi}{c} \hat{\mathbf{z}}$$

Notice that the reciprocal lattice is rotated 30° relative to the real lattice as Fig. 2.3 illustrates.

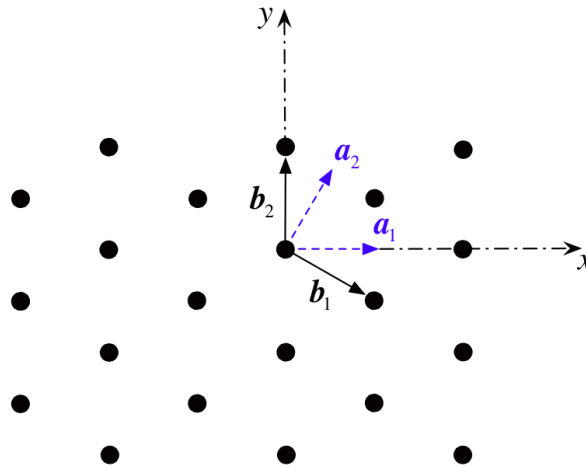


Figure 2.3: Reciprocal hexagonal lattice. Notice how $\mathbf{b}_1 \perp \mathbf{a}_2$ and $\mathbf{a}_1 \perp \mathbf{b}_2$. From the previous equations, note that $|\mathbf{b}_1| = |\mathbf{b}_2| = 4\pi/\sqrt{3}a$.

From diffraction theory, we know that if an incoming x-ray beam $e^{i\mathbf{k}\cdot\mathbf{r}}$ scatters from a volume element dV in a crystal with an outgoing beam $e^{i\mathbf{k}'\cdot\mathbf{r}}$, then constructive interference will occur when the scattering vector $\mathbf{q} = \mathbf{k}' - \mathbf{k}$ is equal to a particular reciprocal lattice vector $\mathbf{G} = h \mathbf{b}_1 + k \mathbf{b}_2 + l \mathbf{b}_3$ ($h, k, l \in \mathbb{Z}$). That is, when

$$\mathbf{q} = \mathbf{G} \quad (2.1)$$

For the case with discrete point scatterers, the scattering amplitude of a single layer becomes

$$\mathbf{E}_{\text{scatter}} \propto \sum_{\{\mathbf{R}_{n,m}\}} e^{-i\mathbf{q}\cdot\mathbf{R}_{n,m}} \quad (2.2)$$

where each $\mathbf{R}_{n,m}$ represents a point in the real lattice. Since the modulation wave vector is in the x-y plane, we can obtain relative amplitudes by only modeling one layer of the real lattice. All layers make the same contribution to the overall intensity. Note that Eq. 2.2 is missing the modulated structure of the Hex-AAA phase. Instead of only having $\mathbf{R}_{n,m}$ as our position vector in the lattice, we must also consider the modulation $\mathbf{u}(\mathbf{R}_{n,m})$ in order to simulate the correct diffraction pattern for this phase. In that case Eq. 2.2 becomes

$$\mathbf{E}_{\text{scatter}} \propto \sum_{\{\mathbf{R}_{n,m}\}} e^{-i\mathbf{q}\cdot(\mathbf{R}_{n,m}+\mathbf{u}(\mathbf{R}_{n,m}))} \quad (2.3)$$

Mathematically, the modulation can be written as

$$\mathbf{u}(\mathbf{R}_{n,m}) = u_0 \hat{\mathbf{z}} \cos(\mathbf{q}_1 \cdot \mathbf{R}_{n,m}) \cos(\mathbf{q}_2 \cdot \mathbf{R}_{n,m}) \quad (2.4)$$

assuming that the shape of the modulation is sinusoidal. Substituting Eq. 2.4 into Eq. 2.3 yields

$$\mathbf{E}_{\text{scatter}} \propto \sum_{\{\mathbf{R}_{n,m}\}} \exp \left[-i \left(q_x a \left(n + \frac{m}{2} \right) + \frac{\sqrt{3}}{2} q_y a m + q_z u_0 \cos(\mathbf{q}_1 \cdot \mathbf{R}_{n,m}) \cos(\mathbf{q}_2 \cdot \mathbf{R}_{n,m}) \right) \right] \quad (2.5)$$

where a general vector \mathbf{q} can be represented as $\mathbf{q} = q_x \hat{\mathbf{x}} + q_y \hat{\mathbf{y}} + q_z \hat{\mathbf{z}}$ and $\mathbf{R}_{n,m} = n \mathbf{a}_1 + m \mathbf{a}_2$. Since we only need one layer in reciprocal space, we set $q_z = |\mathbf{b}_3| = 2\pi/c$ and scale q_x and q_y in units of $4\pi/\sqrt{3}a$. Note that we now have an explicit formula for the amplitude of the modulation. Eq. 2.5 will be the governing equation for the numerical simulation. In order to relate the expression in Eq. 2.5 with the x-ray data in Fig. 2.2, we must multiply Eq. 2.5 by its complex conjugate to obtain the intensity as a function of \mathbf{q} (q_x and q_y). Fig. 2.4 and Fig. 2.5 show plots of intensity vs. q_x and q_y from the numerical simulation. Fig. 2.4 is a close up on the main (001) Bragg peak. Note that there are four small peaks surrounding the main peak a distance of ± 0.046 apart. These are the satellite peaks that indicate the modulation. The distance between the main Bragg peak and the satellites is related to the wavelength of the modulation as previously discussed. Note that this distance matches the separation with the experimental x-ray

data in Fig. 2.2. Fig. 2.5 shows the hexagonal crystal structure when extending the range in \mathbf{q} space.

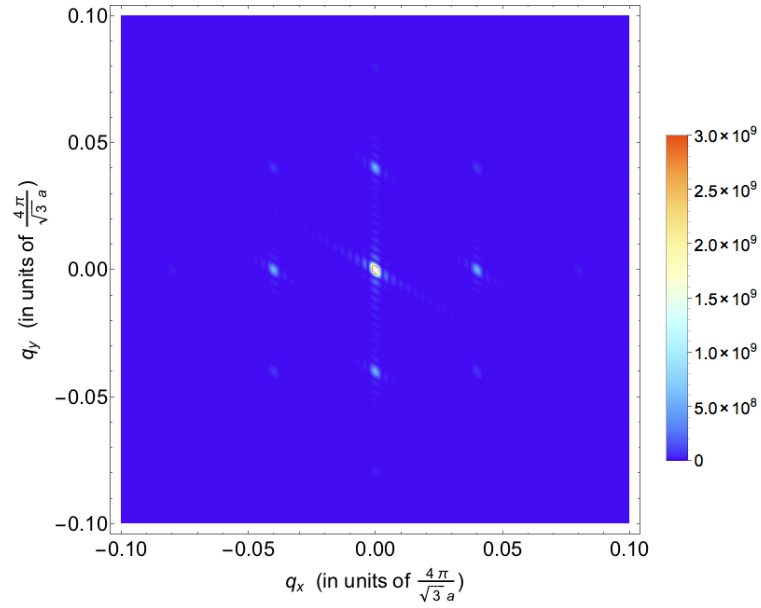


Figure 2.4: Main (001) Bragg peak from the numerical simulation surrounded by satellite peaks due to the modulated structure.

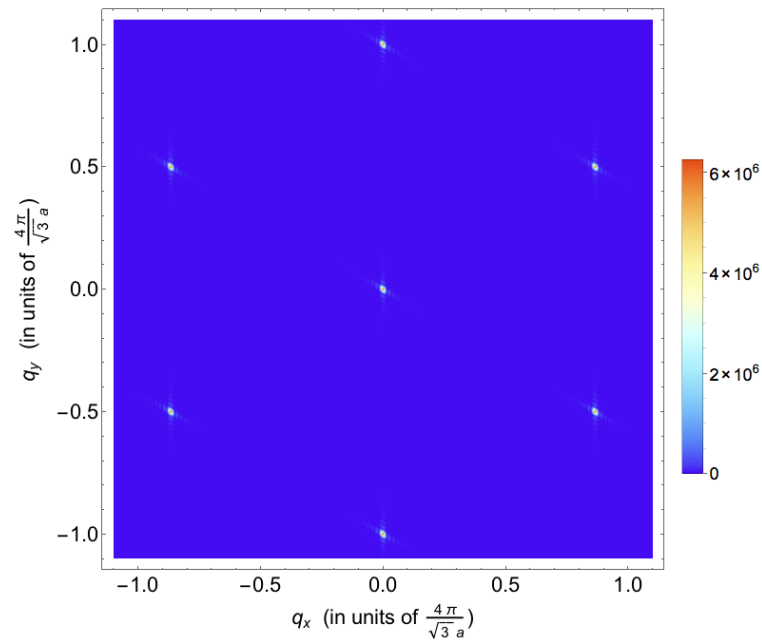


Figure 2.5: Hexagonal structure in \mathbf{q} space from the numerical simulation.

The plot in Fig. 2.4 was simulated with an amplitude ratio of $\frac{u_0}{c} = 0.15$, which corresponds to an amplitude of $u_0 = 0.46$ nm for the modulation. The associated satellite

to main peak ratio then was 0.06. By iterating over many different $\frac{u_0}{c}$ values, we can obtain a relationship between modulation amplitude and satellite to main peak ratio. Fig. 2.6 shows this relationship.

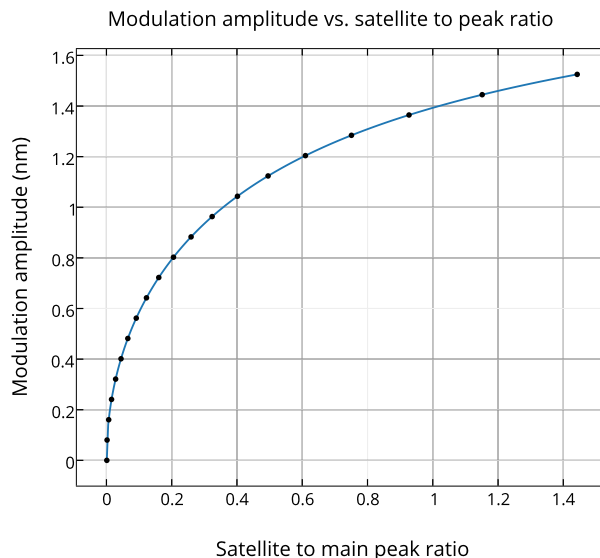


Figure 2.6: Relationship between amplitude of the modulation in the Hex-AAA phase and satellite to main (001) peak ratio. The points represent the numerical data obtained with different $\frac{u_0}{c}$ ratios and the curve is a polynomial fit.

A relationship between modulation amplitude and temperature will be useful to determine the expected size of the modulation at the surface. We can obtain such a relationship from the data in Fig. 2.2b which relates the satellite to peak ratio with temperature. Still, we must make a slight correction to the data presented in Fig. 2.2b because it was taken from a powder sample. In a powder sample, all four satellite peaks are combined into a single satellite peak next to the main peak. Thus, we must divide the values in the y-axis of Fig. 2.2b by 4 in order to compare it with our numerical results. For reasons that will become apparent in the following chapter, a relationship between surface roughness (or standard deviation) and temperature will also be useful. Fig. 2.7 illustrates both of these relationships.

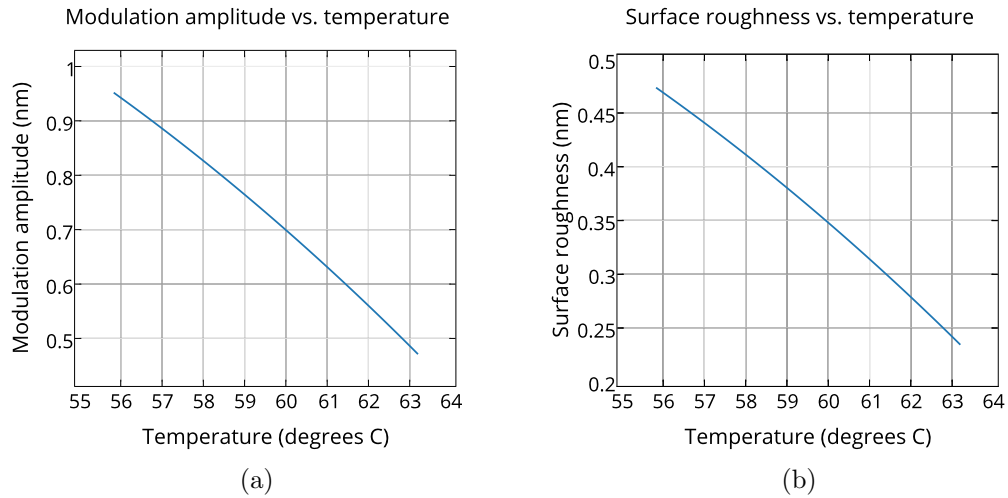


Figure 2.7: (a) prediction for the amplitude of the modulation at the surface as a function of temperature. (b) prediction for the surface roughness as a function of temperature.

Note that the model proposed by Sirota *et al.* in Fig. 2.1b has a sawtooth shape instead of a sinusoidal shape. The entirety of the numerical simulation was repeated with the sawtooth shape. With this particular shape, we should expect slightly higher amplitudes for each temperature, but essentially the same roughness as the sinusoidal model. Given the soft nature of liquid crystals, a sinusoidal modulation without sharp features seems more plausible. Nevertheless, both models were considered and we should expect essentially the same roughness for both shapes. It is reassuring that the roughness prediction is not sensitive to the detailed shape of the modulation.

Fig. 2.7b indicates that in the temperature range of interest (56 °C - 59 °C), we should expect surface roughness values between 0.47 nm and 0.38 nm, respectively. The following chapter discusses the experimental techniques used to determine if the modulation is present or not.

Chapter 3

Experimental techniques

This chapter discusses the experimental methods and techniques used to image the surface of 7O.7. Since we are interested in probing the surface of the films, a scanning microscopy method is a natural consideration. In the first part, we discuss different scanning probe microscopy techniques and explain why non-contact atomic force microscopy (NC-AFM) is suitable for this investigation. In the second part, we explain how to prepare the films and describe the environment where the films reside when imaging the surface. In the last part, we demonstrate a calibration sample scan to illustrate the limits of the instrument and show how sensitive we are at detecting surface features.

3.1 Atomic force microscopy techniques

Atomic force microscopy is a high-resolution type of scanning probe microscopy that can track changes on the order of 0.1 nm in the vertical direction perpendicular to the sample. Non-contact AFM techniques are often used in soft condensed matter and biophysics due to the weak interaction with the surface. Studying the structure of cell membranes and organic compounds is of particular interest because the weak interaction does not distort the structure of the surface. Non-contact atomic force microscopy is the most suitable option for this experiment because 7O.7 films are very soft and delicate. We want to minimize the interaction with the surface as much as possible in order to keep the surface undisturbed.

Other methods such as contact-mode atomic force microscopy and scanning tunneling microscopy are also used to probe surface features, but their interaction with the sample is much stronger. Scanning tunnelling microscopy can provide higher resolutions that can even resolve electron densities of single atoms, but the sample must conduct electricity.

As a consequence, the interaction with the surface increases dramatically. This poses a challenge to many organic-based compounds because establishing a tunnelling current is not always possible. Contact-mode atomic force microscopy uses a sharp tip that applies pressure to the sample in order to image the surface. This method also interacts strongly with the surface and can easily distort it as the tip scans the surface.

Non-contact atomic force microscopy (NC-AFM) will be used to image the surface of freely suspended films of 7O.7. In this mode, a piezoelectric modulator vibrates a cantilever with a sharp tip at its end that is used to scan the surface of a sample. The vibration is driven at the cantilever's resonant frequency. A simple harmonic oscillator can then model the motion of the cantilever with the resonant frequency f_0 equal to

$$f_0 = \frac{1}{2\pi} \sqrt{\frac{k_0}{m}} \quad (3.1)$$

where k_0 represents the spring constant of the harmonic oscillator and m the mass of the cantilever. As the tip approaches the sample, attractive forces, such as the Van Der Waals force, will cause the net force of the oscillator to change. The Van Der Waals force depends on distance from the surface. If the vibration is over a small range of heights, we can make a linear approximation to the force. That linear force with distance is then added to the cantilever's spring force, effectively changing the spring constant. As a consequence, the amplitude and phase of the cantilever's resonant vibration will change. Fig. 3.1 shows the shift in resonance due to the Van Der Waals interaction with the surface. The graph on the left illustrates the interacting forces from the surface as a function of distance from the sample. Note that the highlighted region in green represents the linear regime used in non-contact mode. The graph to the right depicts the shift in resonance due to the change in the spring constant. To track the changes in frequency, there is a laser spot reflected from the top surface of the cantilever into several photodiodes. The signals acquired by the photodiodes are then amplified and processed by sensitive electronics to generate an image of the surface topography[7]. Conventional tips have a radius of 10-20 nm with cantilever dimensions of 30x100 μm . We use super sharp tips with a tip radius of 2-5 nm in order to obtain a higher resolution in the lateral directions.

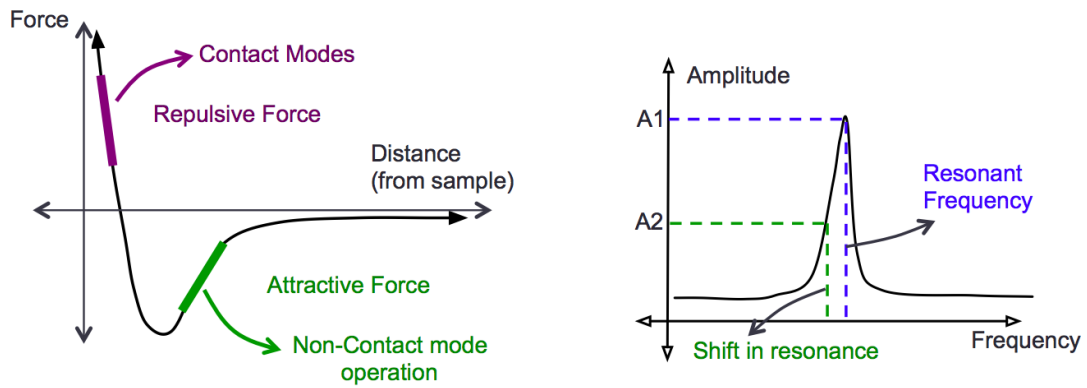


Figure 3.1: The graph on the left illustrates the force as a function of distance from the sample. The graph on the right depicts the shift in resonance due to the Van Der Waals interaction when operating in the non-contact regime highlighted in green.

Fig. 3.2 shows a cartoon version of the AFM operating in non-contact mode.

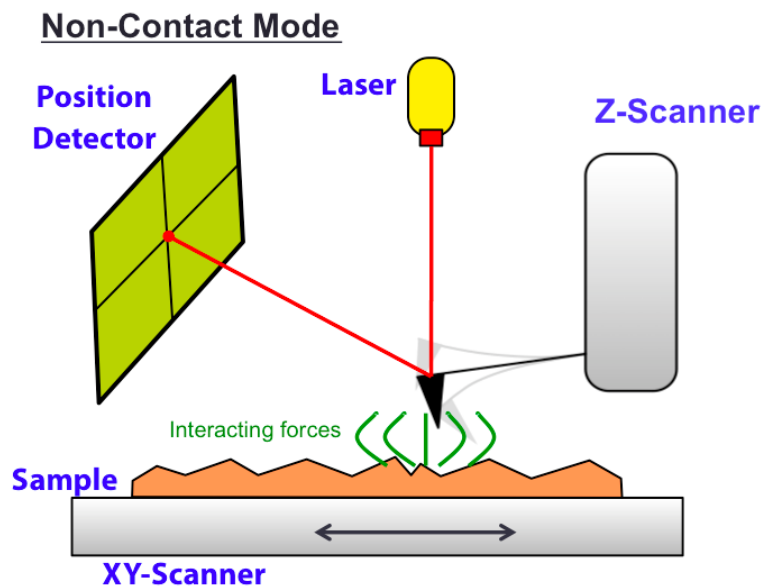


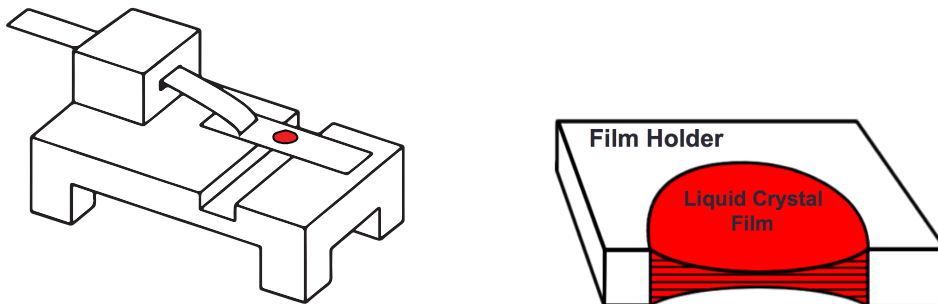
Figure 3.2: Cartoon version of the AFM in non-contact operation.

Note that in Fig. 3.2 the tip of the AFM does not touch the sample at all. Although some tapping may occur, the Van Der Waals interacting forces are long range interactions that do not involve direct contact with the surface. This is the main reason why we use non-contact mode. The surface of 7O.7 is extremely delicate and any form of direct contact will distort it.

3.2 Liquid crystal film assembly

Preparing films of 7O.7 is similar to making a freely suspended soap bubble. This is because the films are prepared in the smectic-A phase, which has similar physical properties to soap. The crystals, which are a solid powder at room temperature, are placed around the hole of the film holder and heated to the smectic-A phase ($\approx 75^\circ\text{C}$). Once in the smectic-A phase, a wiper is used to make a freely suspended film in the hole of the film holder to align the layers parallel to the film holder. After that, the film must have nearly the same thickness throughout the hole. If colored reflections appear, then the film is very thin (on the order of the wavelength of visible light $\approx 500\text{ nm}$) and not uniform enough. If this happens, we must start the process again. Finally, the film is gradually cooled to the Hex-AAA phase in order to obtain high quality crystals. Note that we aim to make thick films so that we are sure that the bulk of the film is in the Hex-AAA phase when cooled.

Since we are probing the surface between 56°C and 59°C , there must be a temperature regulated assembly to monitor and control the temperature of the films. For this particular task, we are using a thermoelectric device mounted to a heating stage that provides adequate heating to our films. The temperature is monitored with a resistance temperature device (RTD) that senses changes of 0.001°C . Fig. 3.3a shows the film stage where the liquid crystal film is located. The thermoelectric device is underneath the stage, and the film holder (Fig. 3.3b) is made of aluminum in order to have proper heat conduction. Notice that the thickness of the film decreases as it gets closer to the center of film.



(a) Film Stage. *Adapted from poster made by Chris Hawley*

(b) Aluminum film holder

Figure 3.3

In addition to the temperature-controlled stage, we also fabricated a custom tip assembly for the tip of the AFM to include temperature control. This allows us to maintain the film and the tip at the same temperature while scanning. This is achieved by having a small thermoelectric device on a modified plate that holds the probe of the AFM where

the tip is located. Without the heated tip, the temperature gradient between the tip and the sample triggers a transition from the Hex-AAA phase to the crystalline-G phase (55 °C - 33 °C), which is not desired. The heated tip is essential to the setup because otherwise the Hex-AAA phase would not be possible to image. This assembly was made at Lawrence University and it is not a conventional piece of equipment encountered in other AFM setups.

3.3 Temperature control

A proportional, integral, and derivative control system (PID) is being used to regulate the temperature of the films to .01 °C. PID controllers are of vital importance and are widely used in industrial control systems. The PID controller calculates an error value, which is the difference between the measured temperature of the films and the desired temperature. The controller attempts to minimize the error by adjusting the voltage that powers the thermoelectric device of the film stage given by

$$v(t) = K_p e(t) + K_i \int_0^t e(t') dt' + K_d \frac{d}{dt} e(t) \quad (3.2)$$

The temperature is measured with the resistance temperature unit (RTD) that is located on top of the film holder. The RTD is linear in our temperature range. The first term in Eq. 3.2 is the proportional gain and it produces an output voltage that is proportional to the error signal. A high proportional gain results in a large change in voltage for a given change in the temperature. The second term in Eq. 3.2 is the integral term and it is proportional to both the magnitude of the error and the duration of the error. The integral term adds the error over time and eliminates the residual steady-state error that occurs with a pure proportional controller. The third term is the derivative term and it accelerates the process towards the desired temperature depending on the slope of the error. If the slope is high, the derivative term will have a stronger contribution and the movement towards the desired temperature will be slowed. This term is not necessary in our setup because the films are cooled/heated very slowly. Thus, for both PID controllers, we set $K_d = 0$. There is also an RTD and a thermoelectric device on the modified assembly of the AFM tip, so in essence, we have two PID setups.

A high-quality 6- $\frac{1}{2}$ digit multimeter is used to measure the resistance of the RTD with a 4-wire measurement. The resistance is then converted to a temperature using the appropriate conversion factor of the RTD. A power supply sends the output signal from Eq. 3.2 in the form of a voltage in order to heat the films via the thermoelectric device. A virtual instrument (VI) in LABVIEW was made in order to make the PID control

algorithm. Both the temperature of the tip and the film are controlled using the same program in LABVIEW. Fig 3.4 shows pictures of the AFM and the AFM head where the tip is located. The orange wires are connected to the RTD and the thermoelectric device in both PID setups.

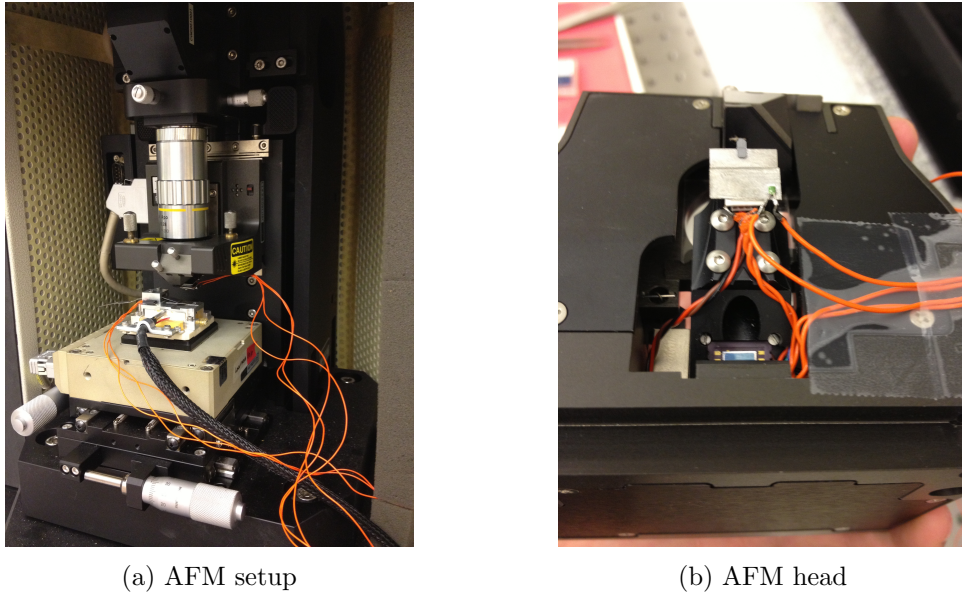


Figure 3.4: (a) AFM setup with flexible wires for the PID controller. (b) AFM head where the tip of the instrument is located. Note that there are two sets of wires in (a): the first set comes from the AFM stage to heat the film and the second set comes from the head of the AFM in order to heat the tip.

3.4 Calibration samples and limits of the AFM

Before discussing the experimental results, we present an image of a silicon carbide calibration sample to display the resolution and limits of the AFM. The silicon carbide sample is essentially a ladder of atomic steps. Each step has a height of 0.75 nm. In some cases, double steps with a corresponding height of 1.50 nm are observed. The steps are atomically sharp, meaning that they are located on the surface. Fig. 3.5a shows the topography of the silicon carbide sample. The changes in color represent variations in height and the scan goes 500 nm in both x and y directions. Fig. 3.5b shows a slice of the variations in height as a function of position. The slice comes from the red rectangle shown in Fig. 3.5a. The plot in the bottom of Fig. 3.5b is a close up of one of the steps from the plot above. Note that the steps presented are double steps.

The resolution in the z-direction (the direction of height changes) of the AFM can resolve much smaller features than the ones presented in Fig. 3.5. Single silicon carbide steps with a height of 0.75 nm were also imaged with the same clarity, and even smaller

changes in height approaching single angstroms can be observed. The lateral resolution in the x and y directions is a bit more limited. The silicon carbide sample presented in Fig. 3.5 is known to have atomically sharp steps on the order of fractions of a nanometer. Nevertheless, the step profile in the bottom of Fig. 3.5b registers a step width of $\approx 4 - 5$ nm. This is not unexpected because the tip of the AFM is not atomically sharp. The tip radius of the probe is about as sharp as the step width measured in the silicon carbide sample. Thus, we should not expect to register changes smaller than $4 - 5$ nm in the x and y directions with extreme clarity. The surface roughness (or standard deviation) of the silicon carbide sample was 0.05 nm in the flat area of constant height between steps.

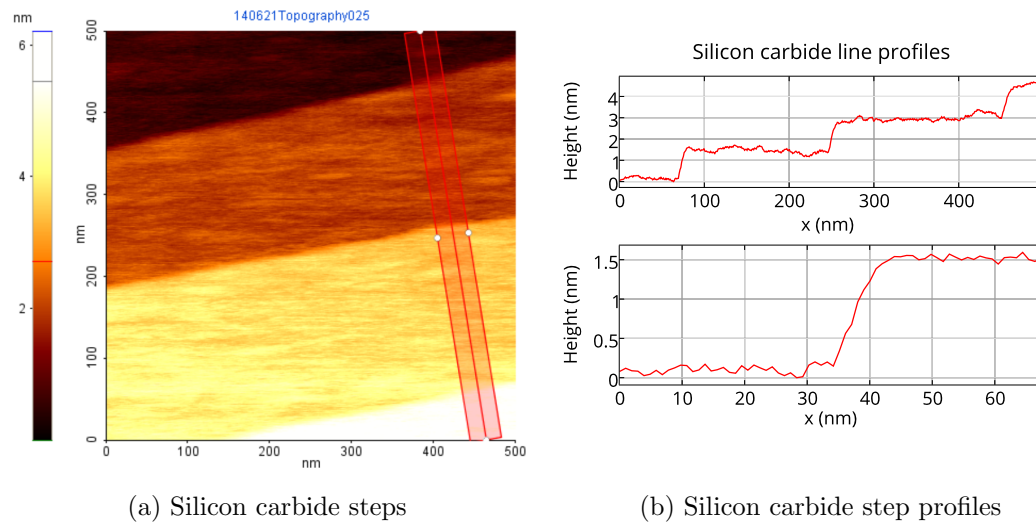


Figure 3.5: Silicon carbide calibration sample data. (a) surface topography of SiC steps on a 500x500 nm block. Note that the changes in color represent changes in height. (b) step profiles of height vs. position from the surface topography in (a).

Chapter 4

Experimental results

The experimental results are presented in the following order: First, we show that the surface differs from the modulated interior because the surface roughness does not match the predictions from chapter 2. Then we show that the step height of single molecular step profiles of 7O.7 corresponds to the upright molecular length. We also demonstrate that the step width is many times greater than the step height. Finally, we show a relationship between step width and temperature that we can correlate with the properties of thin film samples.

4.1 In search of the modulated surface

We carefully measured surface profiles of 7O.7 looking for signs of the modulated structure. Note that the scans from the surface were not expected to resolve the modulation with great detail because the wavelength of the modulation (13.4 nm) calculated in chapter 2 is near the lateral resolution (4 – 5 nm) of the AFM. Nevertheless, the surface roughness should correspond to the value predicted in chapter 2 because the changes in height between 0.94 – 0.76 nm are well within the vertical resolution of the instrument. An average roughness of 0.03 ± 0.02 nm was found in disagreement with the predicted roughness of 0.47 nm to 0.38 nm. Instead, the measured roughness of 7O.7 matches the roughness of the silicon carbide sample presented in Fig. 3.5, which is known to be atomically flat. Fig. 4.1 illustrates one of the featureless scans of the surface with a line profile from the scan. Note that the variations in height are on the order of picometers. At this point, the AFM is reaching its limits and the line scan in Fig. 4.1 may actually represent noise from the instrument. From these results, we can conclude that the surface does reconstruct because the measured roughness is far below the predicted

roughness that matches the modulated structure of the interior. Instead, it corresponds to the roughness of the atomically flat silicon carbide sample.

A natural question to consider might be: What is the surface phase? If it is liquid crystalline, then the most natural phase to consider is the smectic-F phase because it appears in thin films between 56.00 °C and 59.00 °C as shown in Fig. 1.3.

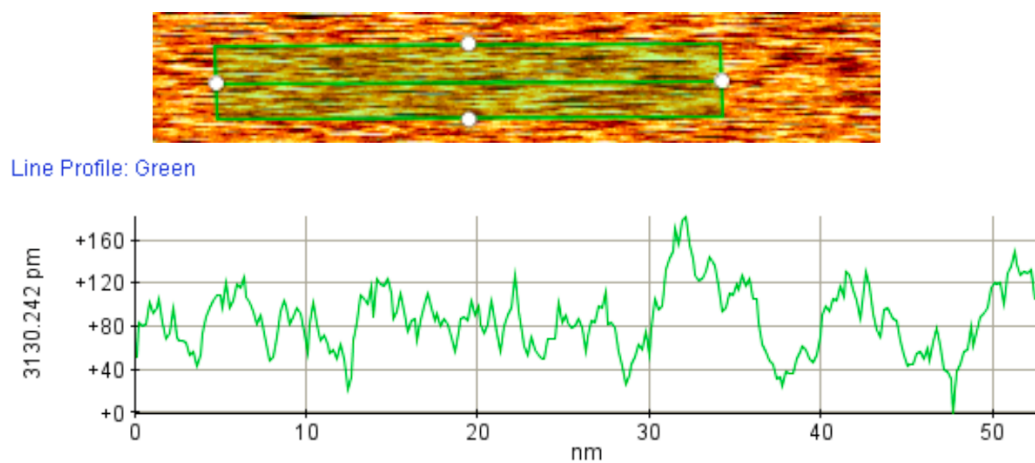


Figure 4.1: Topography strip of the surface of 7O.7 in the Hex-AAA phase and a line profile that registers the changes in height of the strip. Data was taken at T=56.00 °C. This scan had a roughness of 0.04 nm. Expected roughness for a modulated surface at this temperature was 0.47 nm.

As previously discussed, the smectic phases form a layered structure in which the molecules are oriented and free to move within each layer. The smectic-F phase fits this description, but the orientation of the molecules is not perpendicular to the layers as in the smectic-A phase. The molecules tilt by an angle such that the thickness of a tilted layer is 2.75 nm instead of the 3.05 nm of an upright layer. Fig 4.2 illustrates the difference.

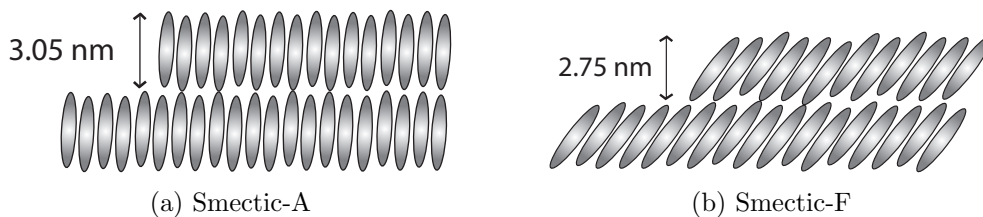


Figure 4.2: Smectic-A and smectic-F molecular steps. For imaging purposes, the only difference between these phases is the height of the molecular steps.

4.2 Molecular steps

Molecular steps of 7O.7 were imaged to try to determine if the molecules were tilted. Fig 4.3 shows a single molecular step of 7O.7 taken at 56.00 °C. Note that the step height does not correspond to the tilted step (2.75 nm) of the smectic-F phase. Instead, the step height agrees with the upright molecular length of 7O.7. More than 40 scans were collected at different temperatures between 56.00 °C and 59.00 °C and a step height of 3.0 ± 0.1 nm was obtained. An interesting feature of the scan in Fig. 4.3 is the difference between the step width and the step height. The step height corresponds to a single molecular step (3.0 nm) while the step width (≈ 120 nm) is many times larger. The fitted red curve will be explained in detail in the following chapter.

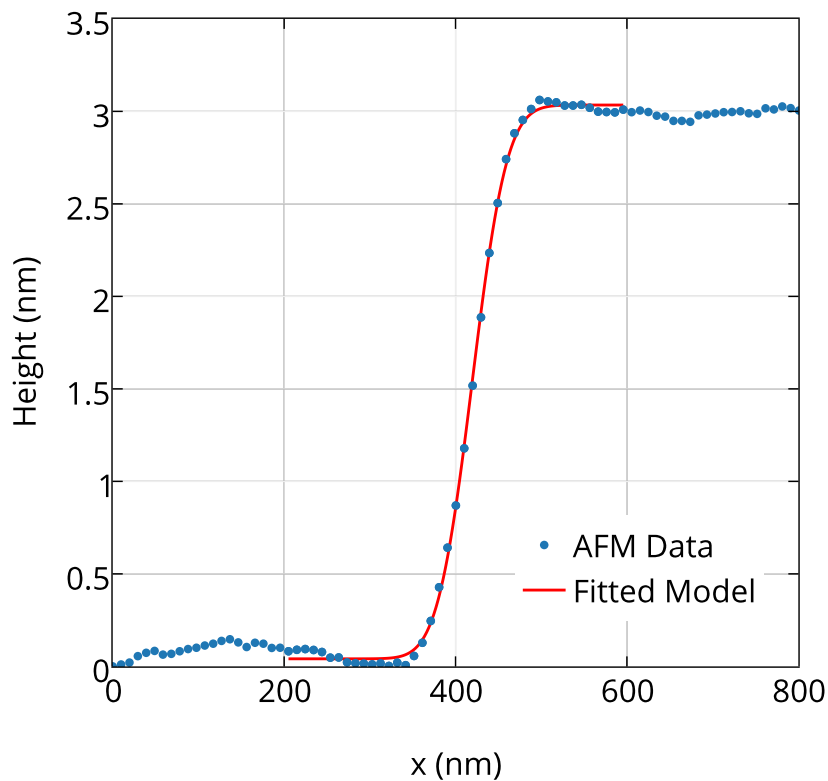


Figure 4.3: Molecular step profile of 7O.7 at 56.00 °C. The height of the step does not correspond to the tilted step of the smectic-F phase. Instead, the height corresponds to the upright molecular length of 7O.7. Note that the step width (≈ 120 nm) is quite large compared to the step height (3.0 nm).

4.3 Temperature-dependent step width

In addition to the preceding results, we find that the step width changes with temperature. Fig. 4.4 shows step profiles imaged at various temperature values with their corresponding widths. From the figure, it is clear that the width of the step is decreasing as the temperature increases. Fig. 4.5 shows the relationship between step width and temperature.

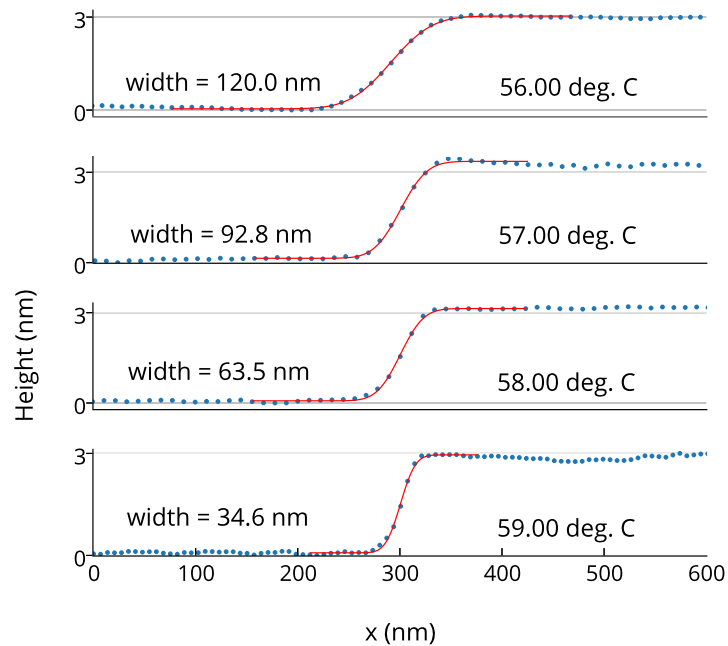


Figure 4.4: Step profiles at different temperatures. Note that the step width decreases as the temperature increases. Also note that the height of the steps stays constant for all temperatures.

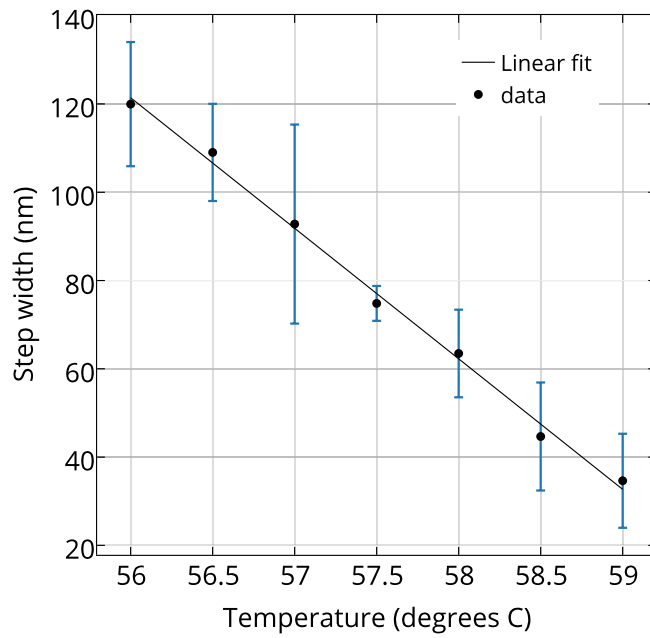


Figure 4.5: Step width as a function of temperature of all the collected step profiles. Note that this relationship matches the one in Fig. 4.4 where the step width increases as the temperature decreases.

The fact that the steps are very wide suggests that incomplete layers are not on the surface. Instead, the steps may originate from edge-dislocations (ending layers) in the interior, and the surface phase is only covering the dislocation. Fig. 4.6 illustrates the model we propose for the reconstructed surface.

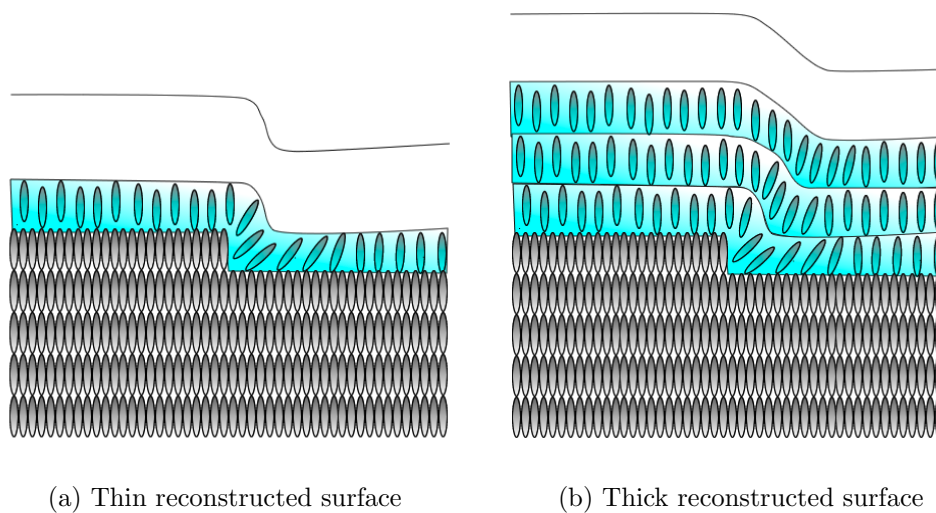


Figure 4.6: Surface reconstruction model. Note that the dislocation that gives birth to the steps originates in the interior of the film. (a) thin reconstructed surface with only a few layers will result in a sharper step. (b) thicker reconstructed surface with many layers will result in a wider step.

The results from Fig. 4.5 indicate that as the temperature decreases, the thickness of the reconstructed surface increases according to the model in Fig. 4.6. The following chapter discusses the model in greater detail.

The experimental results can be summarized as follows:

1. The surface reconstructs because there is no sign of a modulated structure. Instead, the surface is very flat (surface roughness = 0.03 ± 0.02 nm) because it matches the roughness of the atomically flat silicon carbide sample.
2. The step height (3.0 ± 0.1 nm) corresponds to the upright molecular length of 7O.7.
3. The steps are extremely wide compared to the step height suggesting that the steps are not on the surface. Instead, the steps originate from dislocations in the interior.
4. The step width depends on temperature and varies from 120 nm to 35 nm in a linear fashion as seen in Fig. 4.5 between 56.00 °C and 59.00 °C, respectively.

Chapter 5

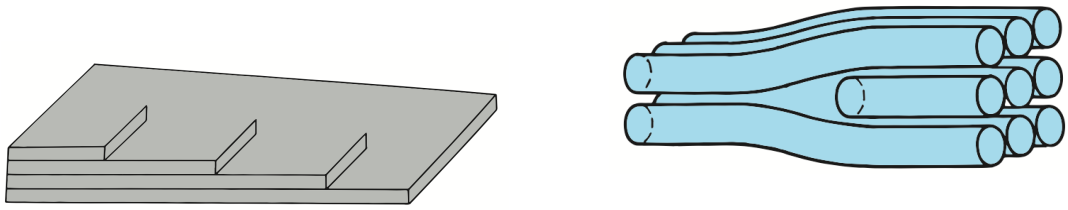
Data analysis and conclusions

In order to analyze the results adequately, we must first discuss the nature of dislocations in liquid crystalline materials. This will provide us with a model to interpret the results in order to obtain quantities such as the thickness of the surface phase. A relationship between the thickness of the surface phase and temperature will then be shown. Finally, we will make an argument suggesting that the surface phase reconstructs into a smectic-F phase.

5.1 Dislocation theory

Dislocations arise naturally in both crystals and liquid crystalline materials. Idealized systems that are infinite in size with a single ordering or arrangement throughout the entire material are not found in nature. Instead, systems are always finite in size and physical boundaries set constraints that force the system to restructure or deviate from the idealized arrangement. The meniscus in Fig. 3.3b, for example, forces the thickness of the sample to decrease as it approaches the center of the film. As a consequence, some of the layers close to the edge of the film must terminate in order to satisfy this constraint. We use this to our advantage to image step profiles of ending layers close to the edge of the film.

Each dislocation in the film has an associated energy that deviates from the idealized minimum energy configuration. Still, the features of the dislocation both in crystals and liquid crystals are such that they minimize their overall energy. Crystals minimize their energy by expelling edge-dislocations (or ending layers) to the surface[8], while liquid crystals force edge-dislocations to the middle of the material[9]. Fig. 5.1 illustrates the difference.



(a) Crystalline edge-dislocation *Adapted from [10]*

(b) Liquid crystalline edge-dislocation *Adapted from [10]*

Figure 5.1: (a) crystals minimize energy by expelling edge-dislocations to the surface. (b) liquid crystals minimize energy by forcing edge-dislocations to the middle (minimizes surface energy).

Edge-dislocation features in crystals are quite different from edge-dislocations encountered in liquid crystals. Edge-dislocations in crystals are atomically sharp where the step width of ending layers at the surface is on the order of fractions of a nanometer. On the other hand, the surface profile of an edge-dislocation of a liquid crystal is quite different because surface tension prevents surface layers from forming atomically sharp steps. Instead, the surface profile covers the dislocation originating in the interior in a gradual manner as depicted in Fig. 5.1b. This particular configuration minimizes the overall surface energy of the liquid crystalline material.

5.2 Model

The reconstructed surface can either be crystalline or liquid crystalline. An isotropic liquid reconstruction is highly unlikely because imaging the surface would have been more challenging. We propose a model where the surface reconstructs into a liquid crystalline phase because the step profiles presented in chapter 4 agree with the wide features of liquid crystalline layers covering edge-dislocations as shown in Fig. 5.1b. It is also reasonable to expect a liquid crystalline surface reconstruction because a smectic-F phase forms in thin films at the temperature range we have investigated. Fig. 4.6 shows the reconstructed model we propose for the surface. The gray interior represents the crystalline phase and the light-colored layers on top of the crystalline phase represent the reconstructed liquid crystalline layers. Note that edge-dislocations are forced to the boundary between the crystalline phase and the liquid crystalline phase. In particular, the edge-dislocation at the boundary stems from the crystalline phase. This is because the step height of the step profiles from chapter 4 matches the layer spacing of the Hex-AAA phase (upright molecular length).

There is also a more convincing argument that suggests that the steps of 7O.7 are not crystalline. We imaged a similar liquid crystalline molecule called 4-n-butyloxybenzylidene-4-n-octyloaniline (abbreviated as 4O.8). This material has a stable crystal phase throughout the entire film (including the surface) over a wide temperature range. The crystal phase is called crystalline-B, which is essentially the same as the Hex-AAA phase without the modulation and a different stacking sequence[11]. We found a step width of 16 ± 2 nm which is sharper than the sharpest width found on 7O.7 (35 ± 11 nm) at 59.00 °C. Although not as sharp as the silicon carbide steps ($4 - 5$ nm), the result found on 4O.8 sets a bound on how sharp edge-dislocations in liquid crystalline materials can be. This is because the steps found on 4O.8 are crystalline edge-dislocations that are directly on the surface as Fig. 5.1a illustrates. The fact that the steps of 4O.8 are not atomically sharp might have to do with the flexible nature of the hydrocarbon tails of the molecule in addition to the soft properties of liquid crystals in general. Nevertheless, the step width of 7O.7, especially at lower temperatures, is many times larger than the step width of 4O.8, indicating that the steps are not at the surface of the crystal.

In order to derive a quantitative model to obtain the thickness of the liquid crystalline surface layer, we must consider the elasticity of the layers and the energy requirements to bend and stretch the molecules from their equilibrium positions. In the hypothetical case where it takes an infinite amount of energy to bend the layers, the dislocation in the interior will create a gap where layers adjacent to the dislocation will never meet to cover the gap. In that case, the surface profile will look completely flat with no sign of a dislocation. On the other extreme, if it takes an infinite amount of energy to stretch the layers, then the layers adjacent to the dislocation will quickly meet right where the middle layer ends and there would be no gap in the region of the dislocation whatsoever. The surface profile of this hypothetical case would have an atomically sharp step with half the size of the layer spacing. Fig. 5.2 illustrates the two different extremes.

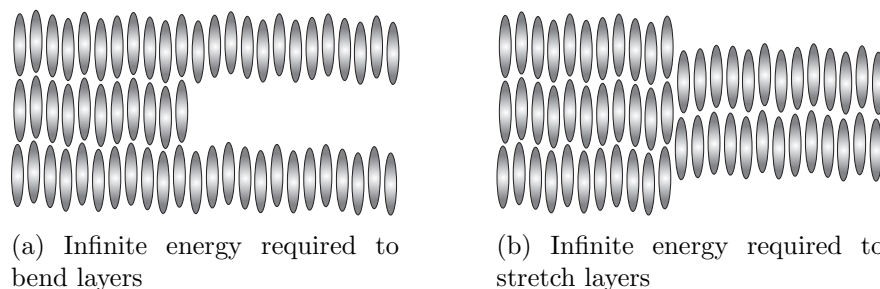


Figure 5.2: Molecular arrangements for two energetic extremes near an edge-dislocation of a liquid crystal.

Neither of these cases is observed in edge-dislocations of liquid crystals. Instead, what we observe is a compromise between the two extremes that minimizes the energy required

to adapt to the dislocation. After minimizing the energy of both distortions, we obtain a relationship between the derivative of the step profile with position given by [10]

$$\frac{\partial u}{\partial x} = \frac{na_0}{4\sqrt{\pi\lambda z}} e^{-x^2/4\lambda z} \quad (5.1)$$

in the limit where many layers are on top of the edge-dislocation. In order to obtain the vertical displacement $u(x)$ that corresponds to the step profile at the surface, we simply integrate the expression in Eq. 5.1 with respect to x to obtain

$$u(x) = \frac{na_0}{4\sqrt{\pi\lambda z}} \int e^{-x^2/4\lambda z} dx \quad (5.2)$$

where na_0 is the magnitude of the Burger's vector[8] that represents the size of the dislocation. In the case where only one layer ends, the Burger's vector has a magnitude of a_0 . Both cases in Fig. 5.2 have $n = 1$. λ is a ratio of elastic constants that involves the amount of energy required to bend and stretch the molecules. For 7O.7, $\lambda \approx 3.05$ nm which corresponds to the layer spacing a_0 . z represents the thickness or number of layers present on top of the dislocation. Fig. 5.3 shows a different representation of the model we introduced in Fig. 4.6. The gray area represents the crystalline interior and the light-colored area represents the liquid crystalline reconstructed layers. Most of the terms in Eq. 5.2 can be identified visually with Fig. 5.3.

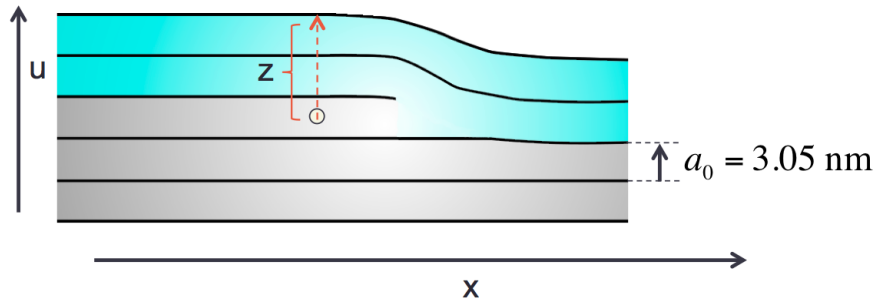


Figure 5.3: Model of the reconstructed surface. The gray area represents the crystalline interior and the light-colored area the liquid crystalline reconstructed layers. z is the height of the surface phase from the edge-dislocation.

There is one main difference between the model we propose and the theory used to obtain the relations in Eq. 5.1 and Eq. 5.2. The equations were derived assuming that the material was purely liquid crystalline, including the edge-dislocation in the interior. Our model has a hybrid structure where the surface is liquid crystalline and the interior is crystalline. In order to account for the difference, we must consider the appropriate

pure liquid crystalline configuration that will generate the surface profile we need. A single ending layer will not work because the height of the step will be half the size of the layer spacing as Fig. 5.2b and Fig. 5.1b illustrate. It takes two ending layers in order to obtain the correct step height from the model in Fig. 5.3. Fig. 5.4 shows a possible configuration that has the step height equal to the layer spacing in agreement with the proposed model. This means that we must set the magnitude of the Burger's vector to $2a_0$.

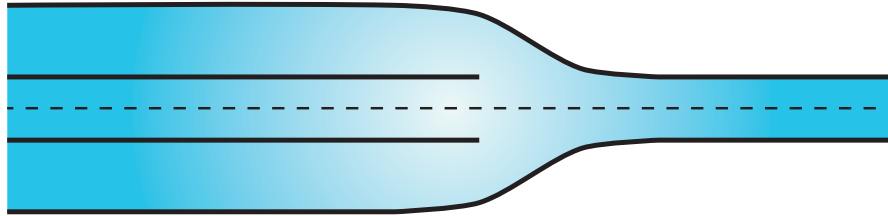


Figure 5.4: Liquid crystalline configuration that has the same step height as the physical model proposed in Fig. 5.3.

5.3 Depth of surface phase vs. temperature

Note that Eq. 5.2 has the same mathematical form as the error function from a normal distribution. Coincidentally, the shape of the surface profile matches the shape of the error function. We use this fact to our advantage because we can obtain quantities such as the standard deviation, which is equal to $\sigma = \sqrt{2\lambda z}$. From this result we can infer the depth of the dislocation (or the thickness of the surface phase) from the width of the step. The fitted curves in the step profiles presented in the previous chapter were obtained using Eq. 5.2 fitting σ as a parameter. The step width was calculated using 4σ to obtain 95 % of the height change in the region of the step.

From the relationship obtained between step width and temperature, we can plot the thickness of the surface phase as a function of temperature using the fact that $z = \sigma^2/2\lambda$. Fig. 5.5 shows the relationship. Note that as the temperature decreases, the thickness of the reconstructed surface increases. At high temperatures between 58 °C and 59 °C there are only a few reconstructed layers ($\approx 13 - 4$) corresponding to a relatively sharp step width between 63 nm and 35 nm, respectively. At low temperatures between 56 °C and 56.5 °C there are many more reconstructed layers ($\approx 50 - 40$) corresponding to a larger step width between 120 nm and 110 nm, respectively. Fig. 4.6b illustrates the difference. The dashed trace in Fig. 5.5 is a quadratic fit.

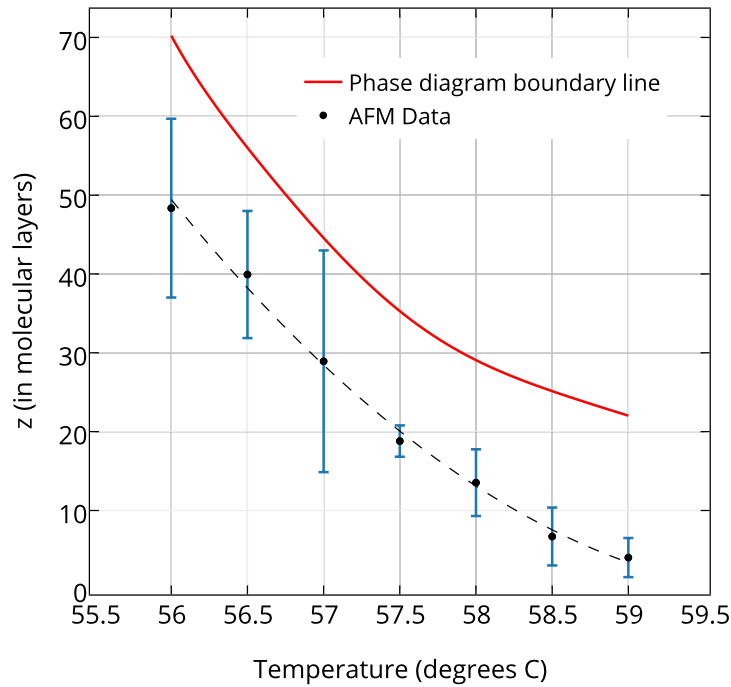


Figure 5.5: Depth of the surface phase as a function of temperature. Note that the dashed trace tracks qualitatively the red boundary of the phase diagram in Fig. 1.3. The vertical axis of the phase diagram was reduced by a factor of two because we only have one freely suspended surface in our model instead of the two free surfaces present in thin films.

5.4 Conclusions

The anomalously large width of the steps and the flatness of the surface lead us to suspect that the surface was reconstructing into a liquid crystalline phase. The sharp step width of 40.8 reassures that the surface is not reconstructing into a crystalline phase because the steps of 70.7 are at least twice as wide. We then proposed a model where the edge-dislocations are forced into the interface between the crystalline phase and the liquid crystalline phase. This happens because crystals minimize their energy by expelling edge-dislocations to the surface while liquid crystals force edge-dislocations to the middle of the material. In particular, the dislocation at the interface stems from the crystalline phase because the height of the steps corresponds to the layer spacing of the Hex-AAA phase. Using a strain model for liquid crystalline layers to estimate the depth of the dislocation, we estimate that the number of reconstructed surface layers decreases from 50 to 4 layers as the temperature increases from 56 °C to 59 °C, respectively.

The red curve in Fig. 5.5 highlights the phase diagram boundary line in Fig. 1.3. This curve represents the limiting thickness for obtaining a pure smectic-F film. Thicker films will form modulated crystalline phases in the bulk as seen in Fig. 1.3. Note that both the red curve and the dashed trace in Fig. 5.5 have a similar thickness dependence with temperature except for an offset of about 20 layers. The boundary line of the phase diagram in Fig. 1.3 has twice the number of layers compared to the red curve in Fig. 5.5 because thin films have two freely suspended surfaces. Our model only has one free surface for the reconstructed liquid crystalline phase. The “missing” free surface is replaced by the interface between the crystalline phase and the liquid crystalline phase. As a consequence, we should not expect a perfect match with the red curve and the dashed trace because the energetics at the interface might affect the maximum number of allowed layers to form. Nevertheless, the thickness of the reconstructed surface clearly matches the behavior of thin films in the smectic-F phase. Hence, this provides strong evidence that the surface is reconstructing into a smectic-F liquid crystalline phase.

This investigation has identified the structure of the interior of the film by imaging the surface profile of molecular steps. That is, we used an imaging technique to infer features as deep as 150 nm from the surface. This method is particularly special because not many physical models can describe what happens inside a material without directly interacting with its interior. In addition, the experimental techniques used in this investigation deserve some recognition. Other experiments have used atomic force microscopy to image liquid crystalline materials[12], but they were placed on top of a plane solid substrate. No one has ever attempted to image freely suspended liquid crystalline films with an atomic force microscope before. Not only have we discovered a surface reconstruction, but we have identified the surface phase and the thickness of the phase as the temperature varies. Many of the questions regarding the surface structure of thick films of 7O.7 have now been answered in this investigation.

References

- [1] Matija Crne Vivek Sharma and Jung Ok Park. What scientists know about jewel beetle shimmer, July 2009. URL https://www.nsf.gov/news/news_summ.jsp?cntn_id=115304.
- [2] Wolfgang Osten and Nadya Reingand. Lcos spatial light modulators: Trends and applications. *Wiley Online Library*, August 2012.
- [3] Peter J. Collings. *Liquid Crystals: Nature's Delicate Phase of Matter*. Princeton Science Library, 1990, p. 9, 96.
- [4] Stephen Morris Philip Hands and Carrie Gillespie. Research at cmmpe — materials — introduction to liquid crystals, 2007. URL <http://www-g.eng.cam.ac.uk/CMMPE/lcintro1.html>.
- [5] E. B. Sirota, P. S. Pershan, and M. Deutsch. Modulated crystalline- B phases in liquid crystals. *Phys. Rev. A*, 36:2902–2913, Sep 1987. doi: 10.1103/PhysRevA.36.2902. URL <http://link.aps.org/doi/10.1103/PhysRevA.36.2902>.
- [6] J. Collett, L. B. Sorensen, P. S. Pershan, J. D. Litster, R. J. Birgeneau, and J. Als-Nielsen. Synchrotron x-ray study of novel crystalline- b phases in heptyloxybenzylidene-heptylaniline (7o.7). *Phys. Rev. Lett.*, 49:553–556, Aug 1982. doi: 10.1103/PhysRevLett.49.553. URL <http://link.aps.org/doi/10.1103/PhysRevLett.49.553>.
- [7] ParkAFM. True non-contactTM mode. URL <http://www.parkafm.com/index.php/park-afm-technology/true-non-contact-mode>.
- [8] Jacques Friedel. *Dislocations*. Addison-Wesley Publishing Company, Inc., 1964, p. 1, 15-16.
- [9] Robert Holyst. Dislocations in lamellar and liquid crystal films: Equilibrium location, edge profiles, and phase transitions. *Phys. Rev. Lett.*, 72:4097–4100, Jun 1994. doi: 10.1103/PhysRevLett.72.4097. URL <http://link.aps.org/doi/10.1103/PhysRevLett.72.4097>.

-
- [10] P. G. de Gennes. *The Physics of Liquid Crystals*. Oxford University Press, second edition, 1993, p. 489, 490.
- [11] D. E. Moncton and R. Pindak. Long-range order in two- and three-dimensional smectic-*b* liquid-crystal films. *Phys. Rev. Lett.*, 43:701–704, Sep 1979. doi: 10.1103/PhysRevLett.43.701. URL <http://link.aps.org/doi/10.1103/PhysRevLett.43.701>.
- [12] M. Maaloum, D. Ausserre, D. Chatenay, G. Coulon, and Y. Gallot. Edge profile of relief 2d domains at the free surface of smectic copolymer thin films. *Phys. Rev. Lett.*, 68:1575–1578, Mar 1992. doi: 10.1103/PhysRevLett.68.1575. URL <http://link.aps.org/doi/10.1103/PhysRevLett.68.1575>.